Bandgap tuning in kerfed metastrips under extreme deformation

Caleb Widstrand, Negar Kalantar, and Stefano Gonella Department of Civil, Environmental, and Geo-Engineering,
University of Minnesota, Minneapolis, MN 55455, USA
Architecture Division, California College of the Arts, San Francisco, CA 94107, USA

The process of kerfing enables planar structures with the ability to undergo dramatic out-of-plane deformation in response to static loads. Starting from flat and stiff sheets, kerfing allows for the formation of a wide variety of unconventional free-form shapes, making the process especially attractive for architectural applications. In this work, we investigate numerically and experimentally the bandgap behavior of densely cut kerfed strips. Our study reveals a rich landscape of bandgaps that is predominantly ascribable to the activation of resonant sub-units within the kerf unit cells. We also document how the extreme deformability of the strips under twisting and bending loads, enhanced by the meandering cut pattern, can serve as a bandgap tuning mechanism.

Kerfing (or relief cutting) is a perforation process consisting of introducing an intricate, periodic pattern of cuts, referred to as a kerf, in a thin structure in a fashion aimed at deliberately increasing its compliance [1, 2]. Kerfing can be performed via laser or water-jet cutting on a variety of material platforms, including composites, such as medium-density fiberboard (MDF), and metals like aluminum or steel. The spatial periodicity makes the design of kerf patterns easily achievable via automatic generation algorithms [3]. By removing solid material and leaving behind a network of interconnected slender elements, kerfing endows an initially flat, homogeneous and relatively stiff sheet with an excess of compliance, making it capable of undergoing dramatic out-of-plane deformation in response to static loads [4].

It is possible to classify kerf patterns according to three archetypal genealogies [5]: 1) linear-cut patterns, involving only parallel cuts and leading to single curvature; 2) offset patterns, in which straight cuts are offset and connected at given angles, allowing double curvature; 3) meandering patterns (the focus of this Letter), featuring tightly interlocking chiral cuts realizable with a variety of cut densities, also conducive to double curvature. The small-scale heterogeneity of densely cut meandering kerfs endows them with extreme deformability that enables morphing into free-form structures. Deformations typically occur within the elastic limit of the material, and are fully reversible upon unloading although, working with composites, it is possible to lock the deformed shapes using epoxy resins. With respect to their ability to undergo large deformation as a result of strategically placed cuts, kerfed sheets are conceptually similar to kirigami structures [6, 7] and structures in which out-ofplane instabilities are promoted by a cut pattern [8, 9]. Though not specifically referred to as kerfing patterns, chiral meandering patterns like the ones studied in this letter have been studied for their in-plane elastic properties [10], where they were found to have a slight auxetic behavior, and for their energy dissipation properties [11].

Kerfed panels are especially appealing for architectural applications, where free-form structures have be-

come increasingly ubiquitous for the design of building facades [12, 13] thanks to their ability to meet simultaneously aesthetic and functional requirements. In this context, kerfed sheets represent a light-weight material that naturally lends itself to being reconfigured in free-form shapes of diverse, pre-designed complexity. An additional benefit lies in the fact that kerfed sheets can be shipped flat and deformed on-site before installation, with major implications for transportation and logistics.

The periodic microstructure of kerfs allows classifying them as examples of elastic phononic crystals (PCs) and metamaterials [14–18], as well as a special subfamily of perforated plates [19-22]. We therefore expect them to exhibit a whole array of dynamical properties classically observed in PCs, and specifically the ability to open bandgaps [23–27]. The first objective of this study is to assess the effectiveness of kerfed structures as bandgap materials. Recently, significant interest has revolved around the design of tunable structures capable of adjusting their behavior in response to externally applied stimuli. A number of strategies have been proposed, in which the tuning is brought about via electromechanical [28] or magneto-mechanical [29, 30] coupling, or by deformation or buckling [31]. In this vein, the second objective of this study is to assess whether the intrinsic extreme deformability of kerfs can be leveraged as an effective tuning mechanism.

Here we focus our attention on kerfed strips, obtained by tessellating in one dimension a macro-cell consisting of a finite number of kerf cells. This choice is motivated by the extreme deformability and reconfigurability that are achievable working with strips, even under relatively small loads. The deformability of the strips results from the combined effect of the compliance inherently provided by their slenderness and the geometric softening introduced by the kerfing process. Let us model a strip as shown in Fig. 1(b) via 1D tessellation of the three-cell-wide macro-cell with a densely cut kerfing pattern shown in Fig. 1(a). The geometry of the kerf is as follows: cell size $h=1.905\,\mathrm{cm}$, ligament width $w=1.143\,\mathrm{mm}$ and out-of-plane strip thickness 0.762 mm. We assume the

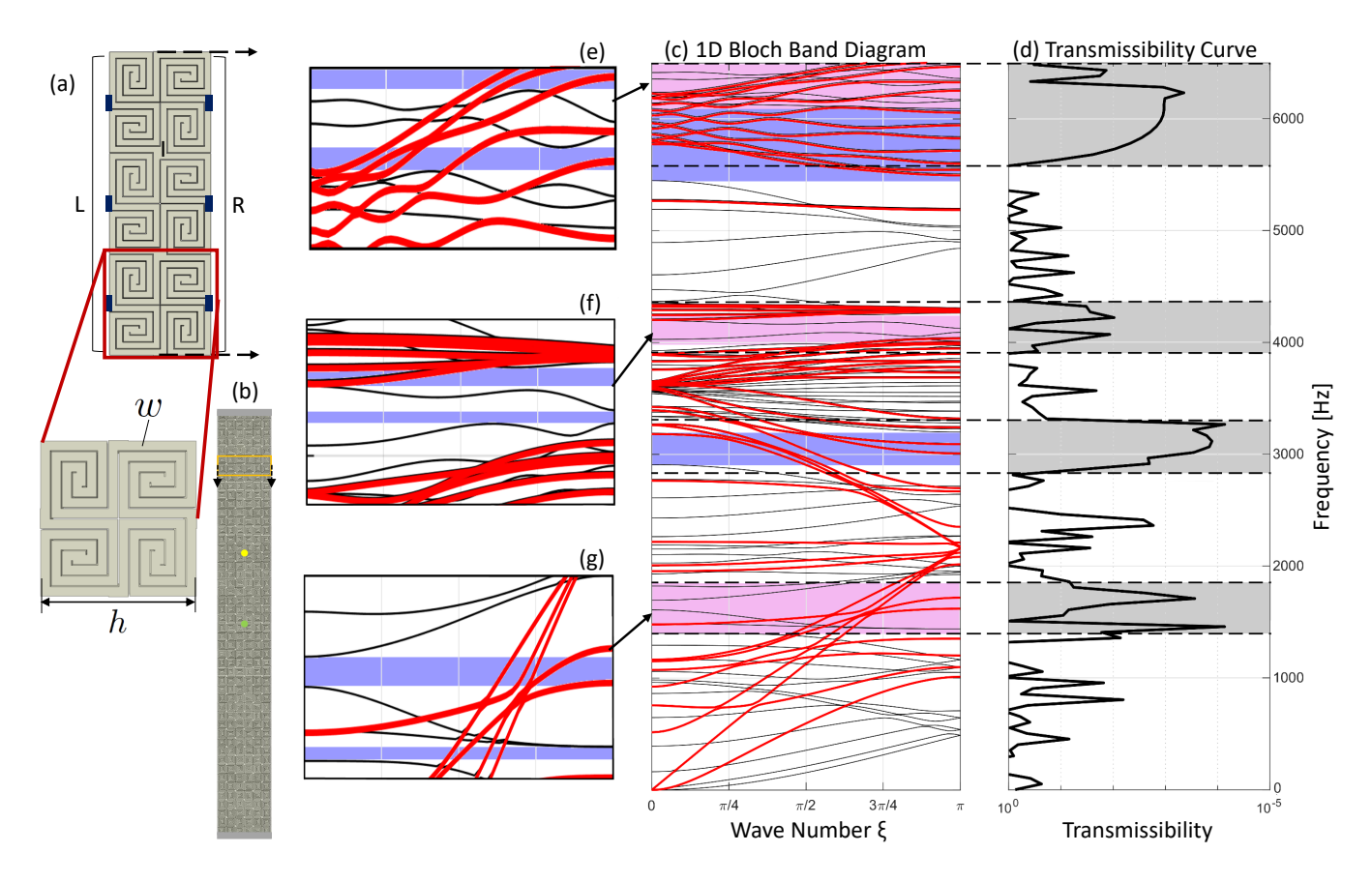


FIG. 1. (a) Macro-cell of densely cut kerfed strip. (b) 3×24 strip with excitation and response sampling points highlighted in green and yellow, respectively. (c) Macro-cell band diagram with main flexural bandgaps highlighted in purple and secondary regions of attenuation in bright pink. (d) Transmissibility curve from harmonic analysis of finite strip. (e-g) Details of secondary attenuation regions revealing clusters of narrow bandgaps separated by nearly-flat modes

material properties of 304 stainless steel: Young's modulus $E = 193 \, \text{GPa}$, Poisson's ratio $\nu = 0.27$ and density ρ $= 7955 \text{ kg/m}^3$. We build a finite element (FE) model of the macro-cell, using a mesh of 8-node isoparametric elements featuring two elements through the thickness. This modeling process is done using the software GMSH [32]. To obtain a band diagram, we follow the canonical steps of 1D Bloch analysis, whereby we apply 1D Bloch conditions between the L and R edge nodes, here confined to the protruding elements marked in blue, leaving the other edges free. We then sweep the scalar non-dimensional wavenumber ξ in the irreducible Brillouin zone, and, for each ξ , we solve an eigenvalue problem involving the reduced stiffness and mass matrices of the macro-cell, vielding the macro-cell dispersion branches. The end result is the band diagram of Fig. 1(c), whose high modal density stems from the ability of the 3D FE model to capture all wave polarizations. Through a comparison of the branches against those obtained from a companion planar model of the macro-cell based on 2D elasticity (details in the SM), we can discriminate between the strictly in-plane modes, marked in red, from those that possess significant out-of-plane character, shown in black. While

no total bandgaps are found in the frequency interval of interest, we recognize two flexural bandgaps, marked in purple, in which flexural modes are evanescent but inplane waves can propagate.

We complement Bloch analysis with a full-scale steadystate analysis on the 3×24 kerfed strip depicted in Fig. 1(b). We prescribe fixed boundary conditions at both ends and we apply a sustained harmonic excitation at the mid point (green dot), sweeping the frequency. The displacement is sampled at the point marked by the yellow dot and normalized by the displacement of the excitation point to construct a curve of transmissibility vs. frequency, plotted in Fig. 1(d). The curve features several regions of attenuation, highlighted in gray. It is clear that only two of these regions can be pinpointed to the major flexural bandgaps discussed above. To elucidate the sources of the other attenuation zones, we zoom in on the corresponding intervals of the band diagram marked in bright pink, detailed in the Fig. 1(e-g) insets. We observe the appearance of clusters of narrower bandgaps, interspersed by nearly flat modes characterized by slow propagation velocities, which, in concert, make these intervals globally unfavorable for transmission.

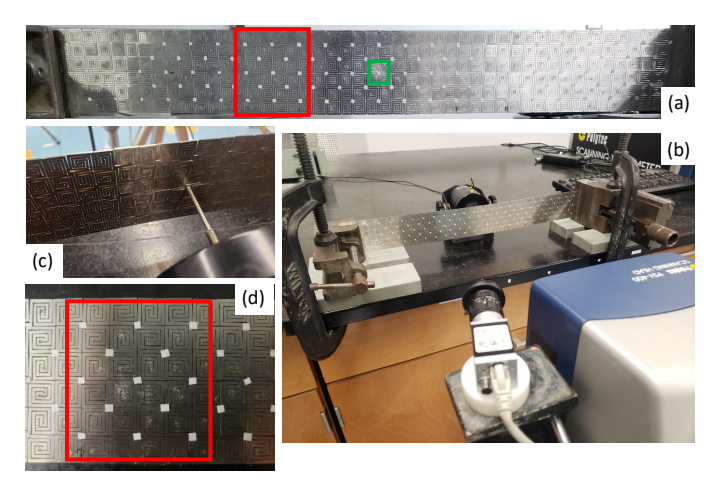


FIG. 2. (a) Flat densely cut kerfed strip with sampling points highlighted in red and excitation point marked in green. (b) Experimental setup showing clamped specimen and laser vibrometer in the foreground. (c) Rear face of specimen showing placement of the shaker. (d) Close-up of sampling region.

From the numerics, we have evinced a rich bandgap landscape and an even richer availability of transmission attenuation intervals, which suggests that densely cut kerfed strips work efficiently as 1D filters. We now seek experimental validation of these findings through a test whose key features are summarized in Fig. 2. The strip shown in Fig. 2(a) is kerfed from a steel plate according to the geometry used for the model. Fig. 2(b) shows the strip ends clamped using a pair of vices and the scanning head of a laser vibrometer (Polytec PSV-400M-3D, used in 1D mode). The excitation is prescribed out-of-plane with a shaker at the point boxed in green on the rear face of the strip (Fig. 2(c)). The red box denotes the response sampling region; in the Fig. 2(d) detail one can appreciate patches of retro-reflective tape applied at the scan points, conveniently located at the connections between cells where uncut areas are more amenable to scanning.

We prescribe a broadband pseudo-random excitation to excite a broad range of frequencies. A drawback of using this kind of signal is that the shaker output energy spectrum decays sensibly with frequency in the interval of interest, thus failing at supplying enough energy at high frequencies. To overcome this, we apply the signal in 2 kHz increments between 0 and 8 kHz, prescribing higher amplitudes in the upper half of the range, such that a roughly equal amount of energy is injected into the system for all frequencies. We measure the out-of-plane velocity at the designated sampling points which span the width of the strip. We average their velocities and normalize this average by the response of the excitation point to construct a measure of velocity transmissibility, plotted against frequency in Fig. 3(a).

We highlight in gray all the regions of attenuation. Comparing against the band diagram juxtaposed in Fig. 3(b) for reference, we observe an overall satisfactory agreement between these intervals and the regions of attenuation predicted by Bloch analysis. Specifically, we can attribute the large drops in transmissibility starting around 2.6 kHz and 5 kHz to the two major flexural bandgaps highlighted in purple, albeit with some discrepancies in the onset frequencies that we will discuss below. Additionally, we can pinpoint the attenuation zone starting around 1.2 kHz and the upper portion of the one starting at 3.2 kHz to the narrow bandgap clusters previously identified in those intervals.

However, the experimental data displays other dips in transmissibility that cannot be attributed to any obvious attenuation mechanism indicated by the band diagram. Some rationale into this discrepancy can be gained by looking at the mode shapes associated with selected spectral points in these ranges. For example, let us consider the two mode shapes at the spectral point highlighted by the yellow dot at 3.6 kHz, plotted in Fig. 3(c) with color map proportional to the normalized out-of-plane displacement. We observe a localization of deflection at the free edges of the macro-cell (the long sides of the strip), deeming these as waveguide modes germane to the 1D geometry of the strip, while the bulk of the strip experiences negligible motion. The black circles superimposed to the figure mark the location of the scan points where we sample the response. The decision to cluster the sampling in the interior of the strip is dictated by practical difficulties encountered in reliably scanning the peripheral portion of the specimen, mostly due to the abnormal lateral deformation and warping exhibited by the edge cells as the result of the cutting process. We recognize that, at this frequency, our scan point selection cannot pick up any response associated with these modes, thus outputting a spurious attenuation zone. Similar considerations can be made about the mode shapes for the spectral points marked by the green and blue dots in Fig. 3(d). While these are definitely bulk modes, they feature nodes (points experiencing negligible displacements) at the scan point locations, which makes them transparent to our sensing strategy. Here, a denser scan would likely detect this modal response and absorb the apparent bandgap conditions, but such refinement would be prohibitive to achieve with a dense cutting pattern.

We also report other discrepancies that appear consistently across experimental takes and that cannot be as easily explained by the morphology of the mode shapes or by the sampling procedure. For instance, we observe frequency downshifts in the experimental data at the onset of both major flexural bandgaps. We believe that the root of these discrepancies lies in defects and geometrical non-idealities embedded in the specimen during the fabrication process, shown in Fig. 3(e), which cause the specimen to deviate from the model. For example, we detect a "waviness" of the cut path that causes a variation in the width of the beams along the kerf pattern. Addi-

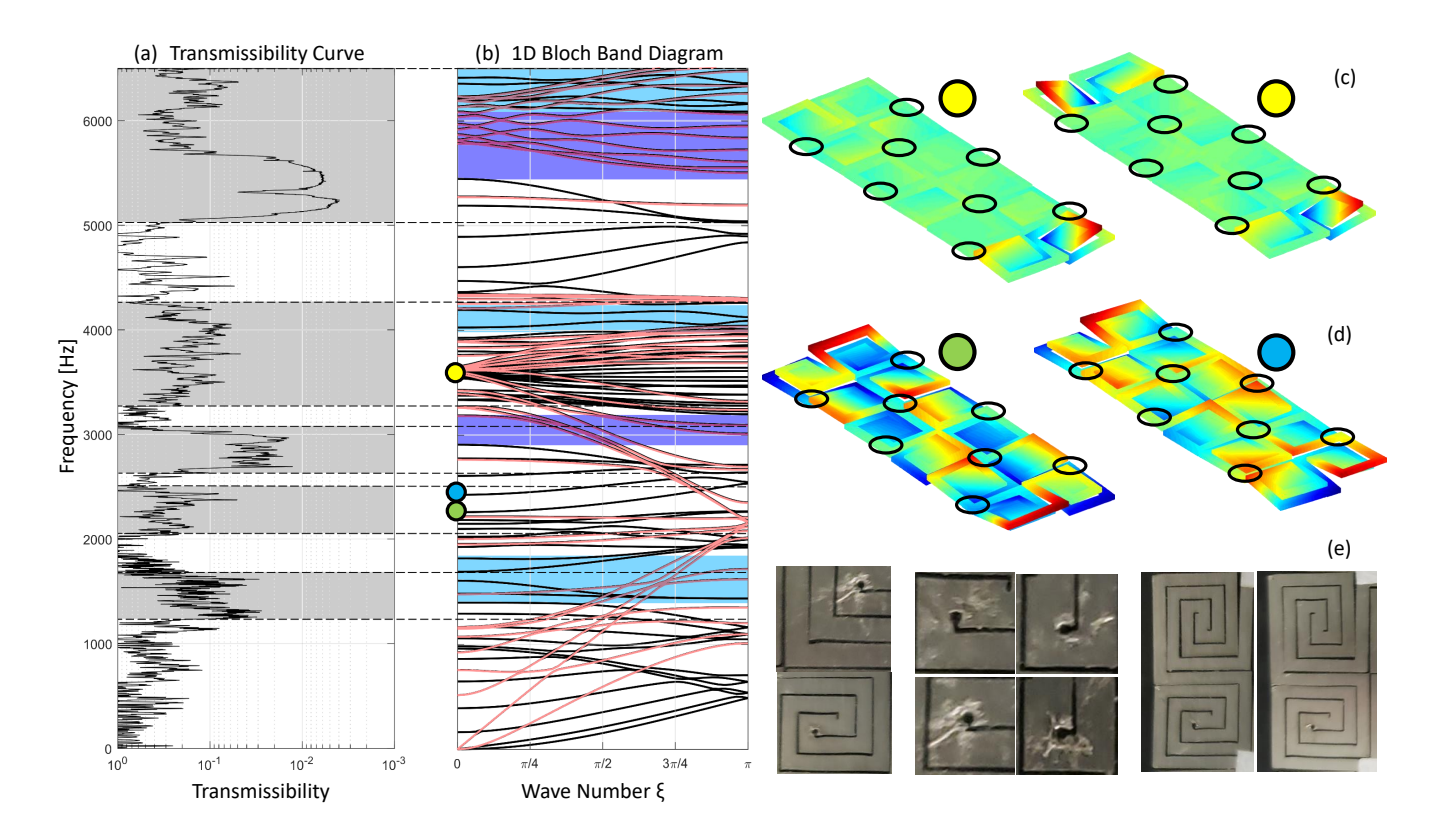


FIG. 3. (a) Experimental transmissibility curve with regions of attenuation highlighted in gray. (b) 1D Bloch band diagram juxtaposed for reference, with out-of-plane modes highlighted in black. (c)-(d) Mode shapes corresponding to experimentally observed frequency ranges of attenuation, with color map corresponding to normalized out-of-plane displacement. Points where the strip is sampled in the experiments, circled in black, featuring negligible displacement. (e) Close-ups of specimen cells, revealing defects and non-idealities.

tionally, we note the presence of fillets where the cutting path terminates, which locally reduce the beam width. Finally, we observe some residual in-plane deformation of the cells located near the edges of the strip, resulting from the lateral pressure exerted during the cutting process. The random distribution of such defects over the specimen inevitably relaxes the assumption of perfect periodicity underpinning the numerical model.

Having established the attenuation behavior of a flat strip, we investigate the possibility to tune its bandgap landscape by subjecting it to a variety of large deformation modes. In our first scenario, we consider a strip twisted by 180° from end-to-end, as shown in Fig. 4(a). In the second case, we bend the strip to form a nearly closed loop, as shown in Fig. 4(b). In both cases, the applied deformation is enabled by a dramatic reconfiguration of the cell's internal features, which experience localized out-of-plane deflections, effectively "popping" out of the strip plane as shown in Figs. 4(c) and (d). We first examine the transmissibility for the twisted case shown in Fig. 4(e). We observe that the attenuation zones, while overall matching those of the flat strip highlighted in gray and recalled in Fig. 4(g), differ in both shape and width. Specifically, the lowest and highest bandgap

openings (around 1 and 5 KHz) display a lower onset compared to their flat strip counterparts, which stretches the intervals of attenuation by the amount marked in pink. Additionally, we observe a merging of the attenuation zones between 2 and 3 KHz at the expense of the major bandgap depth. These results were confirmed by a separate set of tests executed following the same protocols whose results, reported in the SM, show the same qualitative bandgap intervals and correction trends (with minor fluctuations that can be ascribed to some unavoidable residual strains accumulated over deformation cycles). Turning our attention to the bending case of Fig. 4(f), we observe a remarkably similar landscape of modifications in the transmissibility curve, here shaded in green.

While the available data does not allow reaching a definitive explanation for these corrections, we have elements to speculate on the most likely factors behind the observed trends. As the strip deforms, the "pop-out" mechanisms observable in Figs. 4(c) and (d) modify the internal geometry of the cells, thus tuning their resonant characteristics. Incidentally, these modifications are similar between twisting and bending. Since we pinpointed the bandgap formation mechanisms to the resonant be-

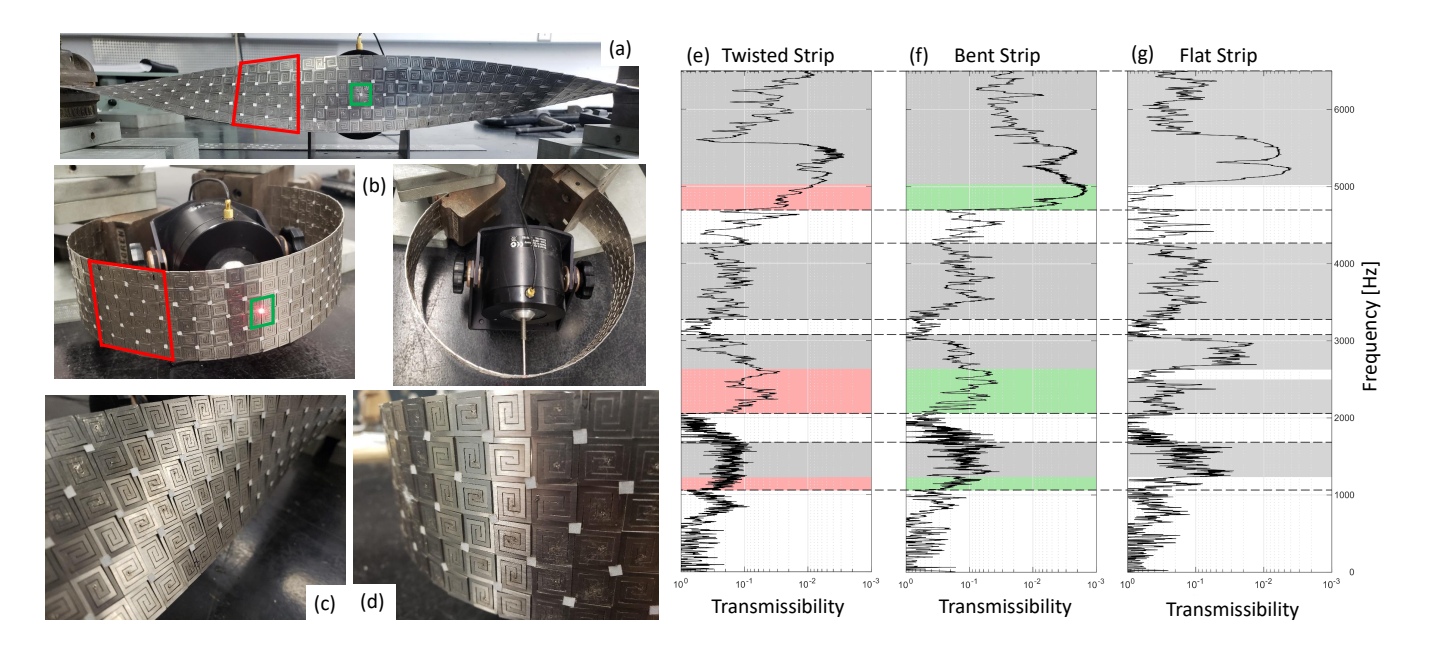


FIG. 4. (a) 180° twisted strip. (b) Bent strip forming nearly closed loop. (c-d) Close-ups of out-of-plane popping mechanisms enabled by the twisting and bending deformations, respectively. (e) Experimental transmissibility curve for twisted strip. Pink regions denote changes in the attenuation zones brought about by twisting. (f) Transmissibility curve for the bent strip, with green regions denoting the corrections induced by bending. (g) Flat strip transmissibility curve.

havior of the internal microstructure, it is reasonable to expect these morphological changes in the resonators to bear an effect on the onset of bandgaps. Another source of correction can lie in the stresses that are developed in the strip upon static deformation. This conjecture is corroborated by a comparison with a small-on-large numerical simulation of the twisted case, reported in the SM; for this, we simulate the twist using a geometrically nonlinear FEM model of the strip, followed by a linear frequency-domain vibration analysis of the twisted strip using the deformed shape as the new reference configuration. Interestingly, the simulation shows negligible tuning. The fact that small-on-large analysis assumes a deformed but unstressed strip suggests that the stresses developed in the physical strip must play a role in correcting the response. Notably, the bandgap widening observed here is reminiscent of that observed in certain metamaterials upon randomization of their resonant microstructure [33]. The spatial non-uniformity of the cell reconfiguration induced by the deformation hints at randomness as a possible co-factor behind these corrections.

In conclusion, we have demonstrated experimentally the rich filtering behavior of kerfed metastrips resulting from the activation of their internal resonant microstructure. This behavior can be modified through the application of extreme twisting and bending, suggesting that the compliance induced by kerfing can be leveraged as a bandgap tuning mechanism.

The authors acknowledge support from the National Science Foundation (EAGER grant CMMI - 1911678).

N.G. also acknowledges partial support from NSF grant CMMI - 1913688. We are grateful to A. Muliana at Texas A&M for useful discussions.

- [1] N. Kalantar and A. Borhani. Informing deformable formworks parameterizing deformation behavior of a non-stretchable membrane via kerfing. *Proceedings of the 23rd CAADRIA Conference*, 2:339–348, 2018.
- [2] D. Mitov, B. Tepavcevic, V. Stojaković, and I. Bajšanski. Kerf bending strategy for thick planar sheet materials. Nexus Network Journal, 21, 10 2018.
- [3] S. Zarrinmehr, M. Ettehad, N. Kalantar, A. Borhani, S. Sueda, and E. Akleman. Interlocked archimedean spirals for conversion of planar rigid panels into locally flexible panels with stiffness control. *Computers & Graphics*, 66, 06 2017.
- [4] R. Chen, C. Turman, M. Jiang, N. Kalantar, M. Moreno, and A. Muliana. Mechanics of kerf patterns for creating freeform structures. Acta Mech, 231:3499–3524, 2020.
- [5] A.-M. Kalama, D. Tzoni, and I. Symeonidou. Kerf bending: A genealogy of cutting patterns for single and double curvature. Proceedings of the 7th International Conference on Geometry and Graphics, 09 2020.
- [6] Y. Zhang, Z. Yan, K. Nan, D. Xiao, Y. Liu, H. Luan, H. Fu, X. Wang, Q. Yang, J. Wang, W. Ren, H. Si, F. Liu, L. Yang, H. Li, J. Wang, X. Guo, H. Luo, L. Wang, Y. Huang, and J. A. Rogers. A mechanically driven form of kirigami as a route to 3d mesostructures in micro/nanomembranes. *Proceedings of the National* Academy of Sciences, 112(38):11757-11764, 2015.
- [7] Y. Tang, Y. Li, Y. Hong, S. Yang, and J. Yin. Pro-

- grammable active kirigami metasheets with more freedom of actuation. *Proceedings of the National Academy of Sciences*, 116(52):26407–26413, 2019.
- [8] Y. Cho, J. Shin, A. Costa, T. A. Kim, V. Kunin, J. Li, S. Lee, S. Yang, H. Han, IS. Choi, and D.J. Srolovitz. Engineering the shape and structure of materials by fractal cut. *Proceedings of the National Academy of Sciences*, 111, 11 2014.
- [9] P. Celli, C. McMahan, B. Ramirez, A. Bauhofer, C. Naify, D. Hofmann, B. Audoly, and C. Daraio. Shapemorphing architected sheets with non-periodic cut patterns. *Soft Matter*, 14, 06 2018.
- [10] W. Zhang, R. Neville, D. Zhang, F. Scarpa, L. Wang, and R. Lakes. The two-dimensional elasticity of a chiral hinge lattice metamaterial. *International Journal of Solids and Structures*, 141-142:254–263, 2018.
- [11] Z. Zhang, F. Scarpa, B. A. Bednarcyk, and Y. Chen. Harnessing fractal cuts to design robust lattice metamaterials for energy dissipation. *Additive Manufacturing*, 46:102126, 2021.
- [12] H. Pottmann. Geometry of architectural freeform structures. Proceedings of the 2008 ACM Symposium on Solid and Physical Modeling, page 9, 1 2008.
- [13] D. Andrade, M. Harada, and K. Shimada. Framework for automatic generation of facades on free-form surfaces. Frontiers of Architectural Research, 6, 06 2017.
- [14] M.S. Kushwaha, P. Halevi, L. Dobrzynski, and B. Djafari-Rouhani. Acoustic band structure of periodic elastic composites. *Physical Review Letters*, 71(13):2022– 2025, 1993.
- [15] M. Sigalas and E. N. Economou. Band structure of elastic waves in two dimensional systems. Solid State Communications, 86(3):141–143, 1993.
- [16] J.S. Jensen. Phononic band gaps and vibrations in oneand two-dimensional mass-spring structures. *Journal of Sound and Vibration*, 266:1053–1078, 10 2003.
- [17] A. Khelif, B. Aoubiza, S. Mohammadi, A. Adibi, and V. Laude. Complete band gaps in two-dimensional phononic crystal slabs. *Physical Review E*, 74:046610, Oct 2006.
- [18] A. Spadoni, M. Ruzzene, S. Gonella, and F. Scarpa. Phononic properties of hexagonal chiral lattices. Wave Motion, 46:435–450, 11 2009.
- [19] T. Slot and W.J. O'Donnell. Effective Elastic Constants for Thick Perforated Plates With Square and Triangular Penetration Patterns. *Journal of Engineering for Indus*try, 93(4):935–942, 11 1971.
- [20] X. Jing and X. Sun. Effect of plate thickness on

- impedance of perforated plates with bias flow. AIAA Journal, 38:1573-1578, 09 2000.
- [21] N.L. Pedersen. Optimization of holes in plates for control of eigenfrequencies. Structural and Multidisciplinary Optimization, 28:1–10, 01 2004.
- [22] S. Hedayatrasa, K. Abhary, M. Uddin, and C.-T. Ng. Optimum design of phononic crystal perforated plate structures for widest bandgap of fundamental guided wave modes and maximized in-plane stiffness. *Journal of the Mechanics and Physics of Solids*, 89, 01 2016.
- [23] Z.-Y. Liu, X. Zhang, Y.-W. Mao, Y.-Y. Zhu, Z. Yang, C. Chan, and P. Sheng. Locally resonant sonic materials. *Science*, 289:1734–6, 10 2000.
- [24] P. Martinsson and A. Movchan. Vibrations of lattice structures and phononic band gaps. The Quarterly Journal of Mechanics and Applied Mathematics, 56, 02 2003.
- [25] S. Gonella and M. Ruzzene. Analysis of in-plane wave propagation in hexagonal and re-entrant lattices. *Journal* of Sound and Vibration, 312:125–139, 04 2008.
- [26] F.-C. Hsu, C.-I. Lee, J.-C. Hsu, T. C. Huang, C.-H. Wang, and P. Chang. Acoustic band gaps in phononic crystal strip waveguides. Applied Physics Letters, 96:051902–051902, 02 2010.
- [27] P. Wang, F. Casadei, S.H. Kang, and K. Bertoldi. Locally resonant band gaps in periodic beam lattices by tuning connectivity. *Phys. Rev. B*, 91:020103, Jan 2015.
- [28] F. Casadei, T. Delpero, A. Bergamini, P. Ermanni, and M. Ruzzene. Piezoelectric resonator arrays for tunable acoustic waveguides and metamaterials. *Journal of Ap*plied Physics, 112, 09 2012.
- [29] O. Bilal, A. Foehr, and C. Daraio. Reprogrammable phononic metasurfaces. Advanced Materials, 29, 08 2017.
- [30] M. Schaeffer and M. Ruzzene. Wave propagation in reconfigurable magneto-elastic kagome lattice structures. *Journal of Applied Physics*, 117:194903, 05 2015.
- [31] P. Wang, F. Casadei, S. Shan, J. Weaver, and K. Bertoldi. Harnessing buckling to design tunable locally resonant acoustic metamaterials. *Physical review letters*, 113:014301, 07 2014.
- [32] C. Geuzaine and J.-F. Remacle. Gmsh: A 3-d finite element mesh generator with built-in pre- and post-processing facilities. *International Journal for Numerical Methods in Engineering*, 79:1309 1331, 09 2009.
- [33] P. Celli and S. Gonella. Manipulating waves with lego® bricks: A versatile experimental platform for metamaterial architectures. Applied Physics Letters, 107, 05 2015.